A novel inverse dynamic model for 3-DoF delta robots☆

Fabio Falezza [a], Federico Vesentini [a,*], Alessandro Di Flumeri [b], Luca Leopardi [b], Gianni Fiori [b], Gianfrancesco Mistrorigo [b], Riccardo Muradore [a]

[a] *Department of Computer Science, University of Verona, Italy*
[b] *SIPRO Srl, Verona, Italy*

ARTICLE INFO

ABSTRACT

Delta Robots belong to a class of parallel robots widely used in industrial production processes, mostly for pick-and-place operations. The most relevant characteristics are the high speed and the extremely favorable ratio between the maximum payload and the weight of the robot itself. A reliable dynamic model is needed to implement torque controllers that reduce unnecessary high accelerations and so mechanical vibrations. The state-of-art inverse dynamic models exploit simplifications in order to facilitate the derivation of the equations of motion and their implementation. In this work, a novel and more rigorous inverse dynamic model is presented which does not rely on simplifications of the kinematic structure. The model has been validated comparing its estimations with real torques data collected moving a Delta Robot D3-1200 by SIPRO Srl; the computational complexity of the algorithm has also been investigated.

1. Introduction

Delta Robots are widely used in industrial applications. Thanks to their rigid structure which allows to achieve more stable functioning, higher velocities and accelerations, and a better positional precision in fast pick-and-place tasks than serial-link manipulators. Furthermore, they are mechanically robust and can move objects of considerable mass and dimension at high speeds [1–5].

The Delta Robot was invented in 1987 by Reymond Clavel and his research team [6]. The robot was originally designed with a mechanical parallel structure with three links, forming a closed kinematic chain connecting a fixed platform to the end-effector. The tool mounted at the end-effector is capable of translating along the Cartesian X, Y and Z axes. Several modifications to the original Delta Robot model have been presented with the intent to increase the degrees of freedom of the end-effector of the robot. For example, a model with four actuated links allowed to rotate the end-effector [7]; or the Hexa Delta robot, whose six kinematic chains arranged by pairs allowed to reach 6-DoF giving the possibility to control the orientation of the end-effector besides its Cartesian position [8].

It is common to refer to the original model with the name 3-DoF Delta Robot, an example shown in Fig. 1. The origin of such name is the presence of three serial kinematic chains with 3 degrees of freedom, which allow the end-effector to move in the three-dimensional workspace. Each kinematic chain consists of two rigid links connected by 2-DoF revolute passive joint. The first link of each chain is actuated by an electric motor, attached to the fixed upper base.

The analysis of the Delta Robot dynamics can be based on complete or approximated models and can exploit different analytical approaches [9], e.g., Principle of Virtual Work, Newton–Euler and Lagrangian formulation.

The presence of only three actuated joints out of nine, the impossibility of finding a closed form for the passive joints that depends only on the actuated ones and a complex kinematic structure with holonomic constraints lead to a complicated mathematical model, that increases the computational burden of its numerical implementation. The recent dynamic models proposed in [10–12] exploit the Lagrangian formulation and simplify the computation by modeling the first link as a homogeneous rod and by considering half of the mass of the second link concentrated at the end of the first link and the other half at the end-effector, in each kinematic chain. This assumption brings to a model relatively easy to handle as it will be shown in Section 2. Unfortunately, it does not take into account a significant part of inertia and potential energy as highlighted in [13,14]. Their approaches consist in adding constant coefficients to be identified, with the intent to compensate for the lack of inertia and potential energy. These coefficients are identified offline through a gray-box approach to match the estimated torques

---

Fig. 1. 3-DoF Delta robot, with the first link highlighted in red, and the second link highlighted in green. Courtesy: Sipro S.r.l. https://www.sipro.vr.it/. (For interpretation of the references to color in this figure legend, the reader is referred to the web version of this article.)

Fig. 2. Geometric representation of a 3-DoFs Delta Robot.

with the actual ones. When an offline approach is not suitable and a precise computation of torques is required, a more rigorous dynamic model must be adopted.

The approaches proposed in [15–18] lead to a complex dynamic model with onerous computations not suitable for a micro-controller to be performed at high frequency. Furthermore, in none of these studies the equations of motion are fully presented with all the terms and derivatives involved. The need to use a symbolic calculus software to calculate the dynamic model explicitly, [19], leads to not-optimized simplifications between the operands, which implies a much more complex model than necessary and increases the difficulty of understanding the model and its computational complexity.

At the best of our knowledge, a rigorous model with every equation taken into account is not present in literature despite the use of Delta Robots in industry for a long time. The dynamic model is adopted in feed-forward control by predicting the torques or within an inverse control architecture [20]. On the other hand, by considering the joints positions, velocities and accelerations to be unknown variables, it is possible to use the model for simulation purposes by solving the forward dynamics.

This paper presents an improvement to the most common simplified dynamic models for 3-DoF Delta Robots by mathematical modeling the second link of every kinematic chain as a homogeneous rod and the first link with generic inertia and position of the center of mass. The computational complexity introduced into the model by this choice will result in an improved and more precise model with respect to actual robots' measurements. The model is derived by computing the dynamics of each variable in the equations of motion, without symbolic calculation software, thus leading to a manageable dynamic model. The friction terms will be neglected, as it has been done in each of the previous works since spherical joints with low friction do not have a high impact on the dynamic behavior of the robot [21]. However, these terms can be added later to the model as usually done for serial-link manipulators [20].

In this paper we present:

- a rigorous inverse dynamic model without simplifications, obtained by exploiting the Lagrangian formulation;
- a complexity analysis of the proposed dynamic model with respect to the state-of-art counterparts, focusing on the trade-off between computational complexity and performance;
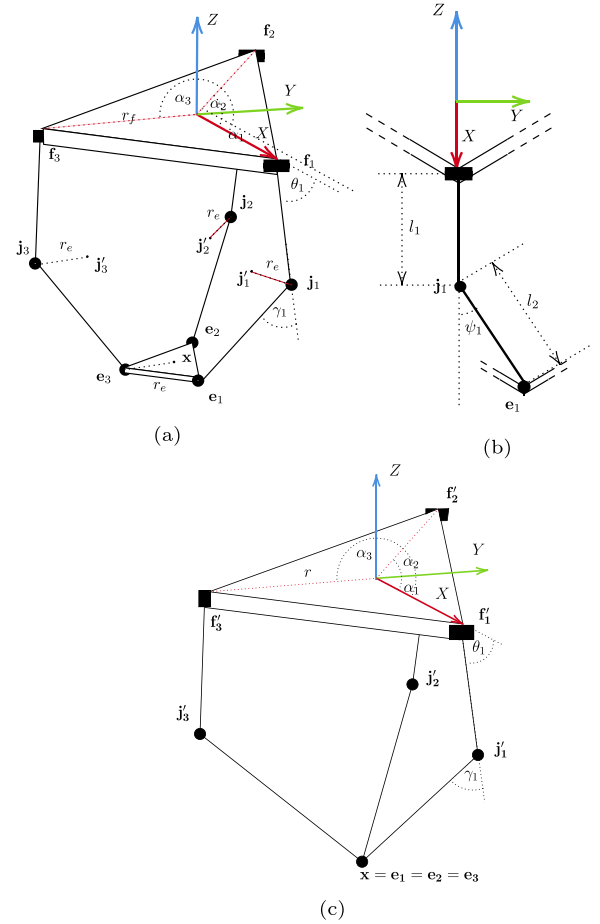
- an experimental verification of the performance of the rigorous model against the simplified one with respect to time series collected on a D3-1200 Delta Robot.

The article is structured as follows: Section 2 recalls the geometric representation of Delta Robots, the used symbols and the approximated dynamics; Section 3 presents the improved mathematical model; in Section 4 the hardware and the experimental setup are described; in Section 5 the result of the complexity analysis are discussed together with the experimental results. Conclusions are drawn in Section 6.

2. The Delta Robot dynamics: Simplified model

A 3-DoF Delta Robot is composed of a moving platform $e_1 - e_2 - e_3$ connected to a fixed base $f_1 - f_2 - f_3$ through three sets of kinematic chains. Each chain consists of two rigid links $\overline{f_i j_i}$ and $\overline{j_i e_i}$, with $i \in \{1, 2, 3\}$, connected by a two-degree passive revolute joint in j_i. Links in the kinematic chains are actuated by three electric motors located at points f_i of the fixed base. The base reference frame $\Sigma_b = \{O; X, Y, Z\}$ is centered in the circumcenter O of rigid platform as shown in Fig. 2. The center of the moving platform is the end-effector, and its position, expressed with respect to the base frame Σ_b, is

$$\boldsymbol{x} = \begin{bmatrix} x \\ y \\ z \end{bmatrix}. \tag{1}$$

The links $\overline{f_i j_i}$ and $\overline{j_i e_i}$ have two 2-DoF spherical joints on j_i and e_i. The proximal and distal links of each kinematic chain have identical length, *i.e.* $l_1 = \|\overline{f_i j_i}\|$ is the length of the actuated link of mass

m_1, $l_2 = \|\overline{j_i e_i}\|$ is the length of the passive links with $i \in \{1, 2, 3\}$. Fig. 1 shows that the passive links are composed of two parallel rods to increase mechanical rigidity. However, for deriving the mathematical model is sufficient to consider just a single rod with total mass m_2 (equal to the sum of the masses of the two parallel rods), as shown in Fig. 2(a). Moreover, $r_f = \|\overline{Of_i}\|$ is the radius of the circle passing from $f_1 - f_2 - f_3$, and $r_e = \|\overline{xe_i}\|$ is the radius of the circle passing from $e_1 - e_2 - e_3$, where $\| \cdot \|$ denotes the Euclidean norm. The angles θ_i with $i \in \{1, 2, 3\}$ represent the joint orientation of actuated links and their values are provided by the motor encoders. The angles γ_i and ψ_i represent the orientation of the passive links as shown in Fig. 2 and are not measured. The angles α_i are the rotation of f_i with respect to O in the $\{X, Y\}$ plane.

In order to treat the end-effector as a point mass whose position is given by (1), we 'horizontally shrink' the entire structure of the robot by r_e, i.e., we consider the geometric representation in Fig. 2(c) which is equivalent to Fig. 2(a) from the dynamics point of view. The radius of the fixed base becomes $r = r_f - r_e$, the motor positions are f_i', the passive joint positions are j_i' and the vertices e_i of the moving platform collapse to x; angles θ_i, γ_i, ψ_i and α_i are preserved as well as the length of the links.

The kinematic structure has to satisfy the following holonomic constraint of rigidity

$$\|x - j_i'\|^2 = l_2^2, \tag{2}$$

cái phương trình constraint này bài nào cũng có

where

$$j_i' = \begin{bmatrix} (r + l_1 c\theta_i) c\alpha_i \\ (r + l_1 c\theta_i) s\alpha_i \\ -l_1 s\theta_i \end{bmatrix}.$$

Eq. (2) is the intersection of three spheres with centers j_i' and radii l_2. From now on, we will use the compact notation $c\alpha$ for $c(\alpha)$, and $s\alpha$ for $s(\alpha)$. Let $\mathcal{L}(q, \dot{q}) = \mathcal{T}(q, \dot{q}) - \mathcal{V}(q)$ be the Lagrangian of the system obtained as difference between kinetic energy $\mathcal{T}$ and potential energy $\mathcal{V}$. According to [10–12,22,23], for deriving the simplified dynamic model $\mathcal{M}_s$ of the robot, we need the following approximations on the kinematic chains shown in Fig. 2:

sử dụng pp Lagrange với các asmpt.

A1: the active links are considered as homogeneous rods of mass m_1, length l_1 and center of mass at $l_1/2$,

A2: the passive links are modeled as two points of mass $m_2/2$ concentrated in j_i' and in x.

These simplifications allow to avoid the inclusion of the passive joint angles γ_i and ψ_i into the generalized coordinates vector q, leading to a system of differential equations relatively simple to handle. The dynamics of a Delta Robot is obtained by solving the constrained Euler–Lagrange equations.

$$\frac{d}{dt}\left(\frac{\partial \mathcal{L}}{\partial \dot{q}}\right) - \frac{\partial \mathcal{L}}{\partial q} = \tau_g + \lambda \frac{\partial \mathcal{F}(q)}{\partial q}, \tag{3}$$

tất cả những tính toán tiếp theo đều giống như 2.6

where

$$\lambda = [\lambda_1 \; \lambda_2 \; \lambda_3]^T$$

are the Lagrange multipliers, τ_g is the generalized force vector acting on the system, $\mathcal{F}(q)$ is the constraint (2) and

$$q = \begin{bmatrix} x \; y \; z \; \theta_1 \; \theta_2 \; \theta_3 \end{bmatrix}^T,$$
$$\dot{q} = \begin{bmatrix} \dot{x} \; \dot{y} \; \dot{z} \; \dot{\theta}_1 \; \dot{\theta}_2 \; \dot{\theta}_3 \end{bmatrix}^T$$

are the generalized coordinates and velocities [24].

The kinetic energy $\mathcal{T}$ of the simplified model $\mathcal{M}_s$ is given by the sum of the kinetic energies of the end-effector $\mathcal{T}_0$, of the actuated links $\mathcal{T}_1$ and of the passive links $\mathcal{T}_2$. Due to assumptions A1 and A2, the inertia terms of the actuated and passive links can be written as

$$\mathcal{I}_1 = \frac{1}{3} m_1 l_1^2, \quad \mathcal{I}_2 = \frac{1}{2} m_2 l_1^2,$$

and since the end-effector $e_1 - e_2 - e_3$ is modeled as a point of mass m_0 in x, the kinetic energy contributions [10,22,23] are then

$$\mathcal{T}_0 = \frac{1}{2} m_0 \|\dot{x}\|^2,$$
$$\mathcal{T}_1 = \frac{1}{2} \mathcal{I}_1 \sum_{i=1}^{3} \dot{\theta}_i^2 = \frac{1}{6} m_1 l_1^2 \sum_{i=1}^{3} \dot{\theta}_i^2,$$
$$\mathcal{T}_2 = \frac{1}{2} \sum_{i=1}^{3} \left(\frac{1}{2} m_2 \|\dot{x}\|^2 + \mathcal{I}_2 \dot{\theta}_i^2\right) = \frac{1}{4} m_2 \sum_{i=1}^{3} \left(\|\dot{x}\|^2 + l_1^2 \dot{\theta}_i^2\right).$$

The potential energy contributions [10,22,23] are

$$\mathcal{V}_0 = m_0 \, gz,$$
$$\mathcal{V}_1 = \frac{1}{2} m_1 \, g \, l_1 \sum_{i=1}^{3} s\theta_i,$$
$$\mathcal{V}_2 = \frac{1}{2} m_2 \, g \sum_{i=1}^{3} (z + l_1 s\theta_i),$$

where g is the gravity acceleration. The computation of the derivatives in Eq. (3) results to

$$\frac{d}{dt}\left(\frac{\partial \mathcal{L}}{\partial \dot{x}}\right) = \left(m_0 + \frac{3}{2} m_2\right) \ddot{x},$$
$$\frac{d}{dt}\left(\frac{\partial \mathcal{L}}{\partial \dot{y}}\right) = \left(m_0 + \frac{3}{2} m_2\right) \ddot{y},$$
$$\frac{d}{dt}\left(\frac{\partial \mathcal{L}}{\partial \dot{z}}\right) = \left(m_0 + \frac{3}{2} m_2\right) \ddot{z},$$
$$\frac{d}{dt}\left(\frac{\partial \mathcal{L}}{\partial \dot{\theta}_i}\right) = \left(\frac{1}{3} m_1 + \frac{1}{2} m_2\right) l_1^2 \ddot{\theta}_i, \qquad i \in \{1, 2, 3\}$$
$$\frac{\partial \mathcal{L}}{\partial x} = 0,$$
$$\frac{\partial \mathcal{L}}{\partial y} = 0,$$
$$\frac{\partial \mathcal{L}}{\partial z} = -\left(m_0 + \frac{3}{2} m_2\right) g,$$
$$\frac{\partial \mathcal{L}}{\partial \theta_i} = -\frac{1}{2} \left(m_1 + m_2\right) g l_1 c\theta_i, \qquad i \in \{1, 2, 3\}.$$

The derivatives with respect to the Cartesian variables, together with the right-hand side of Eq. (3), lead to the following system of second-order differential equations

$$M (\ddot{x} + g) - 2A\lambda = h_{\text{ext}}, \tag{4}$$

with

$$M = \begin{bmatrix} m_0 + \frac{3}{2} m_2 & 0 & 0 \\ 0 & m_0 + \frac{3}{2} m_2 & 0 \\ 0 & 0 & m_0 + \frac{3}{2} m_2 \end{bmatrix},$$

$$\ddot{x} = \begin{bmatrix} \ddot{x} \\ \ddot{y} \\ \ddot{z} \end{bmatrix}, \quad g = \begin{bmatrix} 0 \\ 0 \\ -g \end{bmatrix}, \quad A = \begin{bmatrix} a_{11} & a_{12} & a_{13} \\ a_{21} & a_{22} & a_{23} \\ a_{31} & a_{32} & a_{33} \end{bmatrix},$$

where

$$a_{1i} = x + rc\alpha_i - l_1 c\theta_i c\alpha_i,$$
$$a_{2i} = y + rs\alpha_i - l_1 c\theta_i s\alpha_i, \qquad i \in \{1, 2, 3\}$$
$$a_{3i} = z - l_1 s\theta_i.$$

The vector $h_{\text{ext}} \in \mathbb{R}^3$ represents the external forces applied to the end-effector. The derivatives with respect to the joint variables yield to

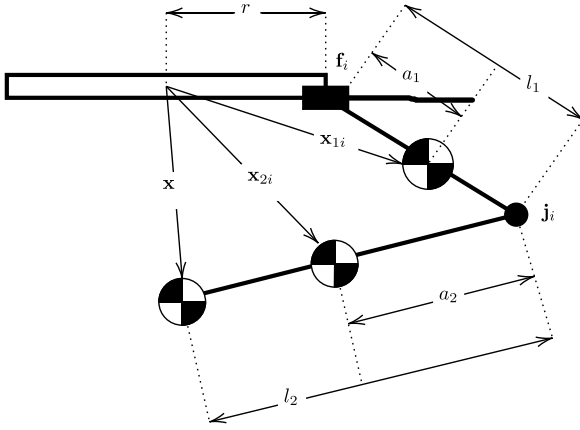$$I\ddot{\theta} + v - 2K\lambda = \tau, \tag{5}$$

Fig. 3. The position of the center of mass of the first link is placed at distance a_1 with respect to f_i along the active link. The position of the center of mass of the second link is placed at distance a_2 with respect to j_i along the passive link.

where τ is the command torques vector and

$$I = l_1^2 \begin{bmatrix} \frac{1}{3}m_1 + \frac{1}{2}m_2 & 0 & 0 \\ 0 & \frac{1}{3}m_1 + \frac{1}{2}m_2 & 0 \\ 0 & 0 & \frac{1}{3}m_1 + \frac{1}{2}m_2 \end{bmatrix},$$

$$\ddot{\theta} = \begin{bmatrix} \ddot{\theta}_1 \\ \ddot{\theta}_2 \\ \ddot{\theta}_3 \end{bmatrix} \quad v = \begin{bmatrix} v_1 \\ v_2 \\ v_3 \end{bmatrix},$$

$$K = \begin{bmatrix} k_{11} & 0 & 0 \\ 0 & k_{22} & 0 \\ 0 & 0 & k_{33} \end{bmatrix}, \quad \tau = \begin{bmatrix} \tau_1 \\ \tau_2 \\ \tau_3 \end{bmatrix}.$$

with

$$v_i = \frac{1}{2}(m_1 + m_2) g\, l_1 c\theta_i,$$

$$k_{ii} = \left(xc\alpha_i + ys\alpha_i + r\right)s\theta_i - zc\theta_i$$

for $i \in \{1, 2, 3\}$. The control torques τ are calculated by solving the system (4) with respect to λ, given the external forces contribution h_{ext}, and then substituting λ into Eq. (5).[1] In the following, we assume $h_{\text{ext}} = [0, 0, 0]^T$.

3. The Delta Robot dynamics: Complete model

$\mathcal{M}_s$ is obtained from very stringent assumptions on the robot links. Modeling the passive links as simple points of mass leads to a noticeable underestimation of the inertia effect and therefore to underestimating the control torques. drawback của p2 và sẽ có những gì ở p3

In this section, a more accurate of 3-DoF Delta Robots $\mathcal{M}_f$ is presented. The active links are a composition of rigid bodies, with center of mass positioned at a point a_1 as shown in Fig. 3. The inertia $\mathcal{I}_1$ is given by the CAD model of the robot. The passive links are no longer mass points, but are modeled as homogeneous rods of mass m_2, length l_2, with center of mass positioned at $a_2 = l_2/2$; since they rotate thanks to passive revolute joints placed in j'_i, their inertia is

$$\mathcal{I}_2 = \frac{1}{3}m_2 l_2^2.$$

---

[1] We point out that in [23] contrary to us, they assume m_2 to be the mass of just one of the two parallel rods constituting the passive links. However, the structure of the equations of motion remains unchanged: the only difference is that m_2 is divided by a factor 2.

Since the end-effector is only capable of translating in the operational space, it can still be modeled as a mass point m_0 placed in x.

For clarity, we introduce the new variables β_i as the sum of the angle of the joints connected to the active links, and the angle of the passive joints whose rotation lies on the same plane of the active link to which it is connected

$$\beta_i \triangleq \theta_i + \gamma_i.$$

Fig. 3 shows the coordinates of the center of mass of each actuated link x_{1i}

$$x_{1i} = \begin{bmatrix} (r + a_1 c\theta_i)c\alpha_i \\ (r + a_1 c\theta_i)s\alpha_i \\ a_1 s\theta_i \end{bmatrix}, \tag{6}$$

the coordinates of the center of mass of each passive link

$$x_{2i} = \begin{bmatrix} (r + l_1 c\theta_i + a_2 c\beta_i c\psi_i)c\alpha_i - a_2 s\psi_i s\alpha_i \\ (r + l_1 c\theta_i + a_2 c\beta_i c\psi_i)s\alpha_i + a_2 c\psi_i s\alpha_i \\ l_1 s\theta_i + a_2 s\beta_i c\psi_i \end{bmatrix}, \tag{7}$$

whereas the coordinate of the end-effector is x.

The corresponding velocity vectors computed by differentiating Eqs. (6), (7), and (1) are showed in (8).

$$\dot{x}_{1i} = \begin{bmatrix} -a_1 \dot{\theta}_i s\theta_i c\alpha_i \\ -a_1 \dot{\theta}_i s\theta_i s\alpha_i \\ a_1 \dot{\theta}_i c\theta_i \end{bmatrix},$$

$$\dot{x}_{2i} = \begin{bmatrix} -\left(l_1\dot{\theta}_i s\theta_i + a_2\dot{\beta}_i s\beta_i c\psi_i + a_2 c\beta_i \dot{\psi}_i s\psi_i\right)c\alpha_i - a_2\dot{\psi}_i c\psi_i s\alpha_i \\ -\left(l_1\dot{\theta}_i s\theta_i + a_2\dot{\beta}_i s\beta_i c\psi_i + a_2 c\beta_i \dot{\psi}_i s\psi_i\right)s\alpha_i - a_2\dot{\psi}_i s\psi_i s\alpha_i \\ l_1\dot{\theta}_i c\theta_i + a_2(\dot{\beta}_i c\beta_i c\psi_i - s\beta_i \dot{\psi}_i s\psi_i) \end{bmatrix}, \quad \dot{x} = \begin{bmatrix} \dot{x} \\ \dot{y} \\ \dot{z} \end{bmatrix}. \tag{8}$$

3.1. Kinetic energy contribution   khá dễ hiểu, chill

In the complete model $\mathcal{M}_f$ we consider also the kinetic energy of the motor rotors $\mathcal{T}_3$. The contributions can be re-written as

$$\mathcal{T}_0 = \frac{1}{2}m_0\|\dot{x}\|^2,$$

$$\mathcal{T}_1 = \sum_{i=1}^{3}\left(\frac{1}{2}m_1\|\dot{x}_{1i}\|^2 + \frac{1}{2}\mathcal{I}_1\dot{\theta}_i^2\right), \quad \text{vì momen quán tính quanh 2 trục là như nhau}$$

$$\mathcal{T}_2 = \sum_{i=1}^{3}\left(\frac{1}{2}m_2\|\dot{x}_{2i}\|^2 + \frac{1}{2}\mathcal{I}_2\dot{\beta}_i^2 + \frac{1}{2}\mathcal{I}_2\dot{\psi}_i^2\right), \tag{9}$$

$$\mathcal{T}_3 = \frac{1}{2}\mathcal{I}_3 k_r^2 \sum_{i=1}^{3}\dot{\theta}_i^2$$

where k_r is the motor gear reduction ratio and $\mathcal{I}_3$ is the inertia of the rotor. For clarification, the following terms are explicitly computed

$$\|\dot{x}_{1i}\|^2 = a_1^2\dot{\theta}_i^2,$$

$$\|\dot{x}_{2i}\|^2 = k_1^2 + a_2^2\dot{\psi}_i^2 s^2\alpha_i + k_1 l_2\dot{\psi}_i s\alpha_i(c\psi_i c\alpha_i + s\psi_i s\alpha_i) + l_1^2\dot{\theta}_i^2 c^2\theta_i + a_1^2 k_2^2 + l_1 l_2\dot{\theta}_i c\theta_i k_2,$$

$$\|\dot{x}\|^2 = \dot{x}^2 + \dot{y}^2 + \dot{z}^2.$$

where k_1 and k_2 group some of the terms for simplicity,

$$k_1 \triangleq l_1\dot{\theta}_i s\theta_i + a_2\left(\dot{\beta}_i s\beta_i c(\psi_i) + c\beta_i\dot{\psi}_i s\psi_i\right), \tag{10}$$

$$k_2 \triangleq \dot{\beta}_i c\beta_i c\psi_i - s\beta_i\dot{\psi}_i s\psi_i. \tag{11}$$

Since it is not possible to express the passive joint angles ψ_i, γ_i as a function of only the actuated joint angles θ_i, we define ψ_i and γ_i as
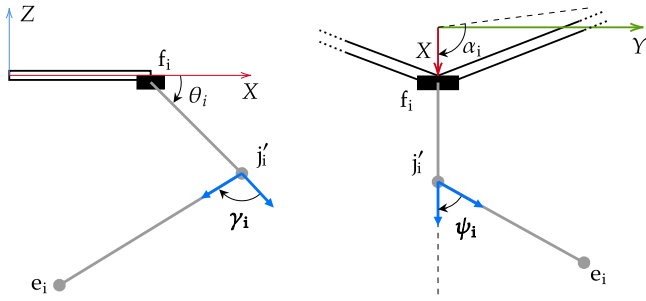
Fig. 4. The passive angles γ_i and ψ_i represented on the planes $\{O; X, Z\}$ and $\{O; X, Y\}$, respectively. The unit vectors of the links projections are drawn in blue. (For interpretation of the references to color in this figure legend, the reader is referred to the web version of this article.)

functions of the generalized coordinates $q = [x \, y \, z \, \theta_1 \, \theta_2 \, \theta_3]^T$ defined in Section 2. They are expressed as

$$\psi_i \triangleq \arccos\left(h_i\right), \quad \gamma_i \triangleq \arccos\left(n_i\right) \tag{12}$$

with

$$h_i = \frac{c\theta_i(xc\alpha_i + ys\alpha_i) - rc\theta_i - l_1 c^2\theta_i}{l_2},$$

muốn tính được 2 góc này phải có thông tin về x,y,z của e-e

$$n_i = \frac{xc\theta_i c\alpha_i - (rc\theta_i + l_1 c^2\theta_i)c^2\alpha_i + zs\theta_i - l_1 s^2\theta_i}{l_2}.$$

Definitions (12) are derived by considering the projections of the links onto the planes $\{O; X, Y\}$ and $\{O; X, Z\}$, respectively. The ψ_i angle is between the projections of $\overline{f_i j_i}$ and $\overline{j_i e_i}$ onto the $\{O; X, Y\}$, and γ_i is the angle between the projections of $\overline{f_i j_i}$ and $\overline{j_i e_i}$ onto $\{O; X, Z\}$ plane, as shown in Fig. 4.

The velocities of the passive joints appearing in Eqs. (9) are given by

$$\dot{\psi}_i = \frac{-1}{\sqrt{1 - h_i^2}}\dot{h}_i, \quad \dot{\gamma}_i = \frac{-1}{\sqrt{1 - n_i^2}}\dot{n}_i. \tag{13}$$

The total kinetic energy contribution $\mathcal{T}$ is the sum of all the previous contributions

$$\mathcal{T} = \sum_{i=0}^{3} \mathcal{T}_i. \tag{14}$$

3.2. Potential energy contribution

The potential energies of the end-effector $\mathcal{V}_0$, of the active links $\mathcal{V}_1$ and the passive links $\mathcal{V}_2$, are

$$\mathcal{V}_1 = m_1 \, g a_1 \sum_{i=1}^{3} s\theta_i, \tag{15}$$

$$\mathcal{V}_2 = m_2 \, g \left(l_1 \sum_{i=1}^{3} s\theta_i + a_2 \sum_{i=1}^{3} s\beta_i c\psi_i\right), \tag{16}$$

$$\mathcal{V}_0 = m_0 \, gz, \tag{17}$$

The total potential energy $\mathcal{V}$ is

$$\mathcal{V} = \sum_{i=0}^{2} \mathcal{V}_i. \tag{18}$$

The rotors do not change position with respect to the Z-axis, therefore it is not necessary to compute their potential energy $\mathcal{V}_3$.

$$\frac{d}{dt}\left(\frac{\partial \mathcal{T}}{\partial \dot{x}}\right) = \frac{1}{2}m_2 \sum_{i=1}^{3} \frac{d}{dt}\frac{\partial \|\dot{x}_{2i}\|^2}{\partial \dot{x}}$$

$$+ \mathcal{I}_2 \sum_{i=1}^{3}\left(\ddot{\beta}_i\frac{\partial\dot{\gamma}_i}{\partial\dot{x}} + \dot{\beta}_i\frac{d}{dt}\frac{\partial\dot{\gamma}_i}{\partial\dot{x}} + \ddot{\psi}_i\frac{\partial\dot{\psi}_i}{\partial\dot{x}} + \dot{\psi}_i\frac{d}{dt}\frac{\partial\dot{\psi}_i}{\partial\dot{x}}\right), \tag{19a}$$

$$\frac{d}{dt}\left(\frac{\partial \mathcal{T}}{\partial \dot{y}}\right) = \frac{1}{2}m_2 \sum_{i=1}^{3} \frac{d}{dt}\frac{\partial \|\dot{x}_{2i}\|^2}{\partial \dot{y}}$$

$$+ \mathcal{I}_2 \sum_{i=1}^{3}\left(\ddot{\beta}_i\frac{\partial\dot{\gamma}_i}{\partial\dot{y}} + \dot{\beta}_i\frac{d}{dt}\frac{\partial\dot{\gamma}_i}{\partial\dot{y}} + \ddot{\psi}_i\frac{\partial\dot{\psi}_i}{\partial\dot{y}} + \dot{\psi}_i\frac{d}{dt}\frac{\partial\dot{\psi}_i}{\partial\dot{y}}\right), \tag{19b}$$

$$\frac{d}{dt}\left(\frac{\partial \mathcal{T}}{\partial \dot{z}}\right) = \frac{1}{2}m_2 \sum_{i=1}^{3} \frac{d}{dt}\frac{\partial \|\dot{x}_{2i}\|^2}{\partial \dot{z}}$$

$$+ \mathcal{I}_2 \sum_{i=1}^{3}\left(\ddot{\beta}_i\frac{\partial\dot{\gamma}_i}{\partial\dot{z}} + \dot{\beta}_i\frac{d}{dt}\frac{\partial\dot{\gamma}_i}{\partial\dot{z}} + \ddot{\psi}_i\frac{\partial\dot{\psi}_i}{\partial\dot{z}} + \dot{\psi}_i\frac{d}{dt}\frac{\partial\dot{\psi}_i}{\partial\dot{z}}\right), \tag{19c}$$

$$\frac{d}{dt}\left(\frac{\partial \mathcal{T}}{\partial \dot{\theta}_i}\right) = \left(\frac{1}{4}m_1 l_1^2 + \mathcal{I}_1 + \mathcal{I}_3 k_r^2\right)\ddot{\theta}_i + \frac{1}{2}m_2\frac{d}{dt}\frac{\partial\|\dot{x}_{2i}\|^2}{\partial\dot{\theta}_i}$$

$$+ \mathcal{I}_2\left(\ddot{\beta}_i\left(1 + \frac{\partial\dot{\gamma}_i}{\partial\dot{\theta}_i}\right) + \dot{\beta}_i\frac{d}{dt}\left(\frac{\partial\dot{\gamma}_i}{\partial\dot{\theta}_i}\right)\right). \tag{19d}$$

3.3. Delta Robot inverse dynamics

The dynamics of a Delta Robot is obtained by solving the constrained Euler–Lagrange equations of the Lagrangian of the system in (3). By expliciting the terms we get

$$\frac{d}{dt}\left(\frac{\partial \mathcal{T}}{\partial \dot{q}}\right) - \frac{d}{dt}\left(\frac{\partial \mathcal{V}}{\partial \dot{q}}\right) - \frac{\partial \mathcal{T}}{\partial q} + \frac{\partial \mathcal{V}}{\partial q} = \tau_g + \lambda\frac{\partial \mathcal{F}(q)}{\partial q}. \tag{20}$$

with

$$\frac{d}{dt}\left(\frac{\partial \mathcal{V}}{\partial \dot{q}}\right) = 0, \tag{21}$$

since there is no dependency on $\dot{q}$ in $\mathcal{V}$.

The time derivative of the partial derivatives of the kinetic energy with respect to $\dot{q}$ are showed in (19). The partial derivatives of the kinetic energy with respect to q are

$$\frac{\partial \mathcal{T}}{\partial x} = \frac{1}{2}m_2 \sum_{i=1}^{3}\frac{\partial\|\dot{x}_{2i}\|^2}{\partial x} + \mathcal{I}_2\sum_{i=1}^{3}\left(\frac{\partial\dot{\gamma}_i}{\partial x}\dot{\beta}_i + \dot{\psi}_i\frac{\partial\dot{\psi}_i}{\partial x}\right),$$

$$\frac{\partial \mathcal{T}}{\partial y} = \frac{1}{2}m_2 \sum_{i=1}^{3}\frac{\partial\|\dot{x}_{2i}\|^2}{\partial y} + \mathcal{I}_2\sum_{i=1}^{3}\left(\frac{\partial\dot{\gamma}_i}{\partial y}\dot{\beta}_i + \dot{\psi}_i\frac{\partial\dot{\psi}_i}{\partial y}\right),$$

$$\frac{\partial \mathcal{T}}{\partial z} = \frac{1}{2}m_2 \sum_{i=1}^{3}\frac{\partial\|\dot{x}_{2i}\|^2}{\partial z} + \mathcal{I}_2\sum_{i=1}^{3}\left(\frac{\partial\dot{\gamma}_i}{\partial z}\dot{\beta}_i + \dot{\psi}_i\frac{\partial\dot{\psi}_i}{\partial z}\right),$$

$$\frac{\partial \mathcal{T}}{\partial \theta_i} = \frac{1}{2}m_2\frac{\partial\|\dot{x}_{2i}\|^2}{\partial\theta_i} + \mathcal{I}_2\left(\dot{\gamma}_i\frac{\partial\dot{\gamma}_i}{\partial\theta_i} + \dot{\psi}_i\frac{\partial\dot{\psi}_i}{\partial\theta_i}\right).$$

For what concern the potential energy, we have the following equations

$$\frac{\partial \mathcal{V}}{\partial x} = -m_2 g a_2 \sum_{i=1}^{3}\left(\frac{\partial\gamma_i}{\partial x}c\beta_i c\psi_i - s\beta_i\frac{\partial\psi_i}{\partial x}s\psi_i\right),$$

$$\frac{\partial \mathcal{V}}{\partial y} = -m_2 g a_2 \sum_{i=1}^{3}\left(\frac{\partial\gamma_i}{\partial y}c\beta_i c\psi_i - s\beta_i\frac{\partial\psi_i}{\partial y}s\psi_i\right),$$

$$\frac{\partial \mathcal{V}}{\partial z} = -m_2 g a_2 \sum_{i=1}^{3}\left(\frac{\partial\gamma_i}{\partial z}c\beta_i c\psi_i - s\beta_i\frac{\partial\psi_i}{\partial z}s\psi_i\right) - m_2 \, g,$$

$$\frac{\partial \mathcal{V}}{\partial \theta_i} = -\left(\frac{m_1}{2} + m_2\right)g l_1 c\theta_i +$$

$$- m_2 g a_2\left(\left(1 + \frac{\partial\gamma_i}{\partial\theta_i}\right)c\beta_i c\psi_i - s\beta_i\frac{\partial\psi_i}{\partial\theta_i}s\psi_i\right).$$

The accelerations $\ddot{\psi}_i$ and $\ddot{\gamma}_i$ of the passive joints are given by

$$\ddot{\psi}_i = \frac{-\left(\ddot{h}_i(1 - h_i^2) + h_i\dot{h}_i^2\right)}{(1 - h_i^2)^{3/2}},$$

$$\ddot{\gamma}_i = \frac{-\left(\ddot{n}_i(1 - n_i^2) + n_i\dot{n}_i^2\right)}{(1 - n_i^2)^{3/2}},$$

for $i \in \{1, 2, 3\}$. The partial derivatives of velocities in Eqs. (13) appearing in the equations of motion are

$$\frac{\partial \dot{\gamma}_i}{\partial \dot{x}} = \frac{-1}{\sqrt{1 - n_i^2}} \frac{\partial \dot{n}_i}{\partial \dot{x}}, \qquad \frac{\partial \dot{\psi}_i}{\partial \dot{x}} = \frac{-1}{\sqrt{1 - h_i^2}} \frac{\partial \dot{h}_i}{\partial \dot{x}}, \tag{22}$$

and analogous expressions hold true also for derivatives with respect to $\dot{y}$, $\dot{z}$ and $\dot{\theta}_i$. The derivatives with respect to time of Eqs. (22) are

$$\frac{d}{dt} \frac{\partial \dot{\gamma}_i}{\partial \dot{x}} = -\left(\frac{\partial \dot{n}_i}{\partial \dot{x}} n_i \dot{n}_i + \frac{d}{dt} \frac{\partial \dot{n}_i}{\partial \dot{x}} (1 - n_i^2) \right) \frac{1}{(1 - n_i^2)^{3/2}}, \tag{23}$$

$$\frac{d}{dt} \frac{\partial \dot{\psi}_i}{\partial \dot{x}} = -\left(\frac{\partial \dot{h}_i}{\partial \dot{x}} h_i \dot{h}_i + \frac{d}{dt} \frac{\partial \dot{h}_i}{\partial \dot{x}} (1 - h_i^2) \right) \frac{1}{(1 - h_i^2)^{3/2}}, \tag{24}$$

Similar equations hold for the derivatives with respect to $\dot{y}$, $\dot{z}$ and $\dot{\theta}_i$. ==All these derivatives are involved in the kinetic energy $\mathcal{T}$, while in the potential energy $\mathcal{V}$ we only have derivatives with respect to Cartesian and joint positions of passive angles' positions and velocities,== defined by Eqs. (12) and (13), respectively. Thus, we have

$$\frac{\partial \gamma_i}{\partial x} = \frac{-1}{\sqrt{1 - n_i^2}} \frac{\partial n_i}{\partial x},$$

$$\frac{\partial \psi_i}{\partial x} = \frac{-1}{\sqrt{1 - h_i^2}} \frac{\partial h_i}{\partial x},$$

$$\frac{\partial \dot{\gamma}_i}{\partial x} = -\left(\frac{\partial n_i}{\partial x} n_i^2 + \frac{\partial \dot{n}_i}{\partial x} (1 - n_i^2) \right) \frac{1}{(1 - n_i^2)^{3/2}},$$

$$\frac{\partial \dot{\psi}_i}{\partial x} = -\left(\frac{\partial h_i}{\partial x} h_i^2 + \frac{\partial \dot{h}_i}{\partial x} (1 - h_i^2) \right) \frac{1}{(1 - h_i^2)^{3/2}},$$

where, as before, the same pattern holds true for derivatives with respect to y, z and $\dot{\theta}_i$. The equations of motion also contain the derivatives of $\|\dot{x}_{2i}\|^2$ with respect to generalized coordinates and velocities, shown in (25), where the time derivatives of k_1 and k_2 terms, defined by Eqs. (10) and (11), are

$$\dot{k}_1 = l_1(\ddot{\theta}_i s\theta_i + \dot{\theta}_i^2 c\theta_i) + a_2 (\ddot{\beta}_i s\beta_i c\psi_i + \dot{\beta}_i^2 c\beta_i c\psi_i) +$$
$$+ a_2 \left(c\beta_i(\ddot{\psi}_i s\psi_i + \dot{\psi}_i^2 c\psi_i) - 2\dot{\beta}_i s\beta_i \dot{\psi}_i s\psi_i \right),$$

$$\dot{k}_2 = \ddot{\beta}_i c\beta_i c\psi_i - \dot{\beta}_i^2 s\beta_i c\psi_i +$$
$$- 2\dot{\beta}_i c\beta_i \dot{\psi}_i s\psi_i - s\beta_i(\ddot{\psi}_i s\psi_i + \dot{\psi}_i^2 c\psi_i),$$

the partial derivatives are

$$\frac{\partial k_1}{\partial \dot{x}} = a_2 \left(\frac{\partial \dot{\gamma}_i}{\partial \dot{x}} s\beta_i c\psi_i + \frac{\partial \dot{\psi}_i}{\partial \dot{x}} c\beta_i s\psi_i \right),$$

$$\frac{\partial k_2}{\partial \dot{x}} = \frac{\partial \dot{\gamma}_i}{\partial \dot{x}} c\beta_i c\psi_i - \frac{\partial \dot{\psi}_i}{\partial \dot{x}} s\beta_i s\psi_i,$$

and the total derivatives are showed in (27).

$$\frac{d}{dt} \frac{\partial \|\dot{x}_{2i}\|^2}{\partial \dot{x}} = 2\left(\dot{k}_1 \frac{\partial k_1}{\partial \dot{x}} + k_1 \frac{d}{dt} \frac{\partial k_1}{\partial \dot{x}} \right) + \frac{l_2^2}{2} s^2 \alpha_i \left(\dot{\psi}_i \frac{\partial \dot{\psi}_i}{\partial \dot{x}} + \dot{\psi}_i \frac{d}{dt} \frac{\partial \dot{\psi}_i}{\partial \dot{x}} \right) +$$
$$+ l_2 s\alpha_i \left((\dot{\psi}_i c\psi_i s\alpha_i - \dot{\psi}_i s\psi_i c\alpha_i) \left(\frac{\partial k_1}{\partial \dot{x}} \dot{\psi}_i + k_1 \frac{\partial \dot{\psi}_i}{\partial \dot{x}} \right) \right) +$$
$$+ l_2 s\alpha_i \left((c\psi_i c\alpha_i + s\psi_i s\alpha_i) \left(\frac{d}{dt} \frac{\partial k_1}{\partial \dot{x}} \dot{\psi}_i + \frac{\partial k_1}{\partial \dot{x}} \ddot{\psi}_i + \dot{k}_1 \frac{\partial \dot{\psi}_i}{\partial \dot{x}} + k_1 \frac{d}{dt} \frac{\partial \dot{\psi}_i}{\partial \dot{x}} \right) \right) +$$
$$+ a_2 \left(\dot{k}_2 \frac{\partial k_2}{\partial \dot{x}} + k_2 \frac{d}{dt} \frac{\partial k_2}{\partial \dot{x}} \right) + l_2 l_1 \left(\ddot{\theta}_i c\theta_i \frac{\partial k_2}{\partial \dot{x}} - \dot{\theta}_i^2 s\theta_i \frac{\partial k_2}{\partial \dot{x}} + \dot{\theta}_i c\theta_i \frac{d}{dt} \frac{\partial k_2}{\partial \dot{x}} \right). \tag{25}$$

$$\frac{d}{dt} \frac{\partial \|\dot{x}_{2i}\|^2}{\partial \dot{\theta}_i} = 2\left(\dot{k}_1 \frac{\partial k_1}{\partial \dot{\theta}_i} + k_1 \frac{d}{dt} \frac{\partial k_1}{\partial \dot{\theta}_i} \right) + \frac{l_2^2}{2} s^2 \alpha_i \left(\dot{\psi}_i \frac{\partial \dot{\psi}_i}{\partial \dot{\theta}_i} + \dot{\psi}_i \frac{d}{dt} \frac{\partial \dot{\psi}_i}{\partial \dot{\theta}_i} \right) +$$
$$+ l_2 s\alpha_i \left((\dot{\psi}_i c\psi_i s\alpha_i - \dot{\psi}_i s\psi_i c\alpha_i) \left(\frac{\partial k_1}{\partial \dot{\theta}_i} \dot{\psi}_i + k_1 \frac{\partial \dot{\psi}_i}{\partial \dot{\theta}_i} \right) \right) +$$
$$+ l_2 s\alpha_i \left((c\psi_i c\alpha_i + s\psi_i s\alpha_i) \left(\frac{d}{dt} \frac{\partial k_1}{\partial \dot{\theta}_i} \dot{\psi}_i + \frac{\partial k_1}{\partial \dot{\theta}_i} \ddot{\psi}_i + \dot{k}_1 \frac{\partial \dot{\psi}_i}{\partial \dot{\theta}_i} + k_1 \frac{d}{dt} \frac{\partial \dot{\psi}_i}{\partial \dot{\theta}_i} \right) \right) +$$
$$+ a_2 \left(\dot{k}_2 \frac{\partial k_2}{\partial \dot{\theta}_i} + k_2 \frac{d}{dt} \frac{\partial k_2}{\partial \dot{\theta}_i} \right) + 2l_1(\dot{\theta}_i c^2 \theta_i - 2\dot{\theta}_i^2 c\theta_i s\theta_i) +$$
$$+ l_2 l_1 \left(c\theta_i \left(\dot{k}_2 + \ddot{\theta}_i \frac{\partial k_2}{\partial \dot{\theta}_i} + \dot{\theta}_i \frac{d}{dt} \frac{\partial k_2}{\partial \dot{\theta}_i} \right) - \dot{\theta}_i s\theta_i \left(k_2 + \ddot{\theta}_i \frac{\partial k_2}{\partial \dot{\theta}_i} \right) \right), \tag{26}$$

$$\frac{d}{dt} \frac{\partial k_1}{\partial \dot{x}} = a_2 \left(\frac{d}{dt} \frac{\partial \dot{\gamma}_i}{\partial \dot{x}} s\beta_i c\psi_i + \frac{\partial \dot{\gamma}_i}{\partial \dot{x}} \dot{\beta}_i c\beta_i c\psi_i - \frac{\partial \dot{\gamma}_i}{\partial \dot{x}} s\beta_i \dot{\psi}_i s\psi_i \right)$$
$$+ a_2 \left(\frac{d}{dt} \frac{\partial \dot{\psi}_i}{\partial \dot{x}} c\beta_i s\psi_i - \frac{\partial \dot{\gamma}_i}{\partial \dot{x}} \dot{\beta}_i s\beta_i s\psi_i + \frac{\partial \dot{\psi}_i}{\partial \dot{x}} c\beta_i \dot{\psi}_i c\psi_i \right) \tag{27a}$$

$$\frac{d}{dt} \frac{\partial k_2}{\partial \dot{x}} = \frac{d}{dt} \frac{\partial \dot{\gamma}_i}{\partial \dot{x}} c\beta_i c\psi_i - \frac{\partial \dot{\gamma}_i}{\partial \dot{x}} \dot{\beta}_i s\beta_i c\psi_i - \frac{\partial \dot{\gamma}_i}{\partial \dot{x}} c\beta_i \dot{\psi}_i s\psi_i$$
$$- \left(\frac{d}{dt} \frac{\partial \dot{\psi}_i}{\partial \dot{x}} s\beta_i s\psi_i + \frac{\partial \dot{\psi}_i}{\partial \dot{x}} \dot{\beta}_i c\beta_i s\psi_i + \frac{\partial \dot{\psi}_i}{\partial \dot{x}} s\beta_i \dot{\psi}_i c\psi_i \right). \tag{27b}$$

$$\frac{\partial \|\dot{x}_{2i}\|^2}{\partial \theta_i} = 2k_1 \frac{\partial k_1}{\partial \theta_i} + \frac{l_2^2}{2} \left(\frac{\partial \dot{\psi}_i}{\partial \theta_i} \dot{\psi}_i s^2 \alpha_i + \frac{\partial k_2}{\partial \theta_i} k_2 \right) - 2l_1^2 \dot{\theta}_i^2 c\theta_i s\theta_i$$
$$+ l_2 l_1 \dot{\theta}_i \left(c\theta_i \frac{\partial k_2}{\partial \theta_i} - k_2 s\theta_i \right) +$$
$$+ l_2 s\alpha_i \left(\left(\frac{\partial k_1}{\partial \theta_i} \dot{\psi}_i + k_1 \frac{\partial \dot{\psi}_i}{\partial \theta_i} \right) (c\psi_i c\alpha_i + s\psi_i s\alpha_i) \right)$$
$$+ l_2 s\alpha_i \left(k_1 \dot{\psi}_i \frac{\partial \dot{\psi}_i}{\partial \theta_i} (c\psi_i s\alpha_i - s\psi_i c\alpha_i) \right), \tag{28}$$

where

$$\frac{\partial k_1}{\partial \theta_i} = a_2 \left(s\beta_i \left(\frac{\partial \dot{\gamma}_i}{\partial \theta_i} c\psi_i - \dot{\beta}_i \frac{\partial \psi_i}{\partial \theta_i} s\psi_i - \left(1 + \frac{\partial \gamma_i}{\partial \theta_i} \right) \dot{\psi}_i s\psi_i \right) \right)$$
$$+ a_2 \left(c\beta_i \left(\frac{\partial \dot{\psi}_i}{\partial \theta_i} s\psi_i + \dot{\beta}_i \frac{\partial \gamma_i}{\partial \theta_i} c\psi_i + \frac{\partial \psi_i}{\partial \theta_i} \dot{\psi}_i c\psi_i \right) \right) + l_1 \dot{\theta}_i c\theta_i,$$

$$\frac{\partial k_2}{\partial \theta_i} = c\beta_i \left(\frac{\partial \dot{\gamma}_i}{\partial \theta_i} c\psi_i - \dot{\beta}_i \frac{\partial \psi_i}{\partial \theta_i} s\psi_i - \left(1 + \frac{\partial \gamma_i}{\partial \theta_i} \right) \dot{\psi}_i s\psi_i \right)$$
$$+ s\beta_i \left(\frac{\partial \dot{\psi}_i}{\partial \theta_i} s\psi_i - \dot{\beta}_i \left(1 + \frac{\partial \gamma_i}{\partial \theta_i} \right) c\psi_i - \frac{\partial \psi_i}{\partial \theta_i} \dot{\psi}_i c\psi_i \right).$$

The derivatives with respect to $\dot{y}$ and $\dot{z}$ follow the same pattern. Derivatives about joint variables θ_i and $\dot{\theta}_i$ are given in (26). The partial and total derivatives of k_1 and k_2 terms, defined by Eqs. (10) and (11), are

$$\frac{\partial k_1}{\partial \dot{\theta}_i} = l_1 s\theta_i + a_2 \left(\left(1 + \frac{\partial \dot{\gamma}_i}{\partial \dot{\theta}_i} \right) s\beta_i c\psi_i + s\beta_i \frac{\partial \dot{\psi}_i}{\partial \dot{\theta}_i} s\psi_i \right),$$

$$\frac{\partial k_2}{\partial \dot{\theta}_i} = \left(1 + \frac{\partial \dot{\gamma}_i}{\partial \dot{\theta}_i} \right) c\beta_i c\psi_i - s\beta_i \frac{\partial \dot{\psi}_i}{\partial \dot{\theta}_i} s\psi_i$$

$$\frac{d}{dt} \frac{\partial k_1}{\partial \dot{\theta}_i} = 2l_1 \dot{\theta}_i c\theta_i +$$
$$+ a_2 \left(\left(\frac{d}{dt} \frac{\dot{\gamma}_i}{\partial \dot{\theta}_i} s\beta_i + 2\dot{\beta}_i \left(1 + \frac{\partial \dot{\gamma}_i}{\partial \dot{\theta}_i} \right) c\beta_i \right) c\psi_i \right) +$$
$$+ a_2 \left(c\beta_i \left(\frac{d}{dt} \frac{\partial \dot{\psi}_i}{\partial \dot{\theta}_i} s\psi_i + 2\dot{\psi}_i \frac{\partial \dot{\psi}_i}{\partial \dot{\theta}_i} c\psi_i \right) \right) +$$
$$- \left(l_2 s\beta_i s\psi_i \left(\left(1 + \frac{\partial \dot{\psi}_i}{\partial \dot{\theta}_i} \dot{\psi}_i \right) \dot{\psi}_i + \dot{\beta}_i \frac{\partial \dot{\psi}_i}{\partial \dot{\theta}_i} \right) \right),$$

$$\frac{d}{dt} \frac{\partial k_2}{\partial \dot{\theta}_i} = \left(\frac{d}{dt} \frac{\partial \dot{\gamma}_i}{\partial \dot{\theta}_i} c\beta_i - \frac{\partial \dot{\gamma}_i}{\partial \dot{\theta}_i} \dot{\beta}_i s\beta_i \right) c\psi_i +$$
$$- \frac{\partial \dot{\gamma}_i}{\partial \dot{\theta}_i} c\beta_i \dot{\psi}_i s\psi_i +$$
$$- \left(\dot{\beta}_i c\beta_i \frac{\partial \dot{\psi}_i}{\partial \dot{\theta}_i} + s\beta_i \frac{d}{dt} \frac{\partial \dot{\psi}_i}{\partial \dot{\theta}_i} \right) s\psi_i +$$
$$- s\beta_i \frac{\partial \dot{\psi}_i}{\partial \dot{\theta}_i} \dot{\psi}_i c\psi_i.$$

Finally, we have the derivatives of $\|\dot{x}_{2i}\|^2$ with respect to Cartesian and joint positions. As usual, we only show the partial derivatives with respect to x since those about y and z follow the same pattern. For Cartesian positions, we have

$$\frac{\partial \|\dot{x}_{2i}\|^2}{\partial x} = 2k_1 \frac{\partial k_1}{\partial x} +$$
$$+ \frac{l_2^2}{2} \left(\frac{\partial \dot{\psi}_i}{\partial x} \dot{\psi}_i s^2 \alpha_i + \frac{\partial k_2}{\partial x} (k_2 + l_1 \dot{\theta}_i c\theta_i) \right) +$$

Khuyết điểm:
Có quá nhiều phương trình cần tính
Vẫn chưa take into account influence của Dynamic Gearbox + Friction
Vẫn chưa vip lắm

F. Falezza et al.   *Mechatronics 83 (2022) 102752*

$$+ l_2 s\alpha_i$$

$$\left(\left(\frac{\partial k_1}{\partial x} \ddot{\psi}_i + k_1 \frac{\partial \ddot{\psi}_i}{\partial x} \right) (c\psi_i c\alpha_i + s\psi_i s\alpha_i) \right) +$$

$$+ l_2 s\alpha_i \left(k_1 \dot{\psi}_i \frac{\partial \psi_i}{\partial x} (c\psi_i s\alpha_i - s\psi_i c\alpha_i) \right),$$

where

$$\frac{\partial k_1}{\partial x} = c_2 \left(s\beta_i \left(\frac{\partial \dot{\gamma}_i}{\partial x} c\psi_i - \dot{\beta}_i \frac{\partial \psi_i}{\partial x} s\psi_i - \frac{\partial \gamma_i}{\partial x} \dot{\psi}_i s\psi_i \right) \right) +$$

$$+ c_2 \left(c\beta_i \left(\dot{\beta}_i \frac{\partial \gamma_i}{\partial x} c\psi_i + \frac{\partial \ddot{\psi}_i}{\partial x} s\psi_i + \dot{\psi}_i \frac{\partial \psi_i}{\partial x} c\psi_i \right) \right),$$

$$\frac{\partial k_2}{\partial x} = -s\beta_i \left(\dot{\beta}_i \frac{\partial \gamma_i}{\partial x} c\psi_i + \frac{\partial \ddot{\psi}_i}{\partial x} s\psi_i + \dot{\psi}_i \frac{\partial \psi_i}{\partial x} c\psi_i \right) +$$

$$+ c\beta_i \left(\frac{\partial \dot{\gamma}_i}{\partial x} c\psi_i - \dot{\beta}_i \frac{\partial \psi_i}{\partial x} s\psi_i - \frac{\partial \gamma_i}{\partial x} \dot{\psi}_i s\psi_i \right),$$

whereas, for joint positions, we end up with (28).

The constrained Lagrangian dynamics can thus be written in compact form as

$$2A\lambda = b, \tag{29}$$

where the matrix A and the vectors b and λ are defined as

$$A = \begin{bmatrix} a_{11} & a_{12} & a_{13} \\ a_{21} & a_{22} & a_{23} \\ a_{31} & a_{32} & a_{33} \end{bmatrix}, \qquad \lambda = \begin{bmatrix} \lambda_1 \\ \lambda_2 \\ \lambda_3 \end{bmatrix},$$

$$b = \begin{bmatrix} \frac{d}{dt}\left(\frac{\partial \mathcal{T}}{\partial \dot{x}}\right) - \frac{\partial \mathcal{T}}{\partial x} + \frac{\partial \mathcal{V}}{\partial x} \\ \frac{d}{dt}\left(\frac{\partial \mathcal{T}}{\partial \dot{y}}\right) - \frac{\partial \mathcal{T}}{\partial y} + \frac{\partial \mathcal{V}}{\partial y} \\ \frac{d}{dt}\left(\frac{\partial \mathcal{T}}{\partial \dot{z}}\right) - \frac{\partial \mathcal{T}}{\partial z} + \frac{\partial \mathcal{V}}{\partial z} \end{bmatrix},$$

with

$$a_{1i} = x + rc\alpha_i - l_1 c\theta_i c\alpha_i,$$
$$a_{2i} = y + rs\alpha_i - l_1 c\theta_i s\alpha_i,$$
$$a_{3i} = z - l_1 s\theta_i,$$

for $i \in \{1, 2, 3\}$. The solutions of the system (29) is $\lambda = \frac{1}{2} A^{-1} b$, and the command torques are obtained by substituting λ into the following equation

$$\tau = n(q, \dot{q}, \ddot{q}) + c(q, \dot{q}) + g(q) - 2K(q)\Lambda, \tag{30}$$

where

$$n(q, \dot{q}, \ddot{q}) = \begin{bmatrix} \frac{d}{dt}\left(\frac{\partial \mathcal{T}}{\partial \dot{\theta}_1}\right) \\ \frac{d}{dt}\left(\frac{\partial \mathcal{T}}{\partial \dot{\theta}_2}\right) \\ \frac{d}{dt}\left(\frac{\partial \mathcal{T}}{\partial \dot{\theta}_3}\right) \end{bmatrix}, \quad c(q, \dot{q}) = \begin{bmatrix} -\frac{\partial \mathcal{T}}{\partial \theta_1} \\ -\frac{\partial \mathcal{T}}{\partial \theta_2} \\ -\frac{\partial \mathcal{T}}{\partial \theta_3} \end{bmatrix},$$

$$g(q) = \begin{bmatrix} \frac{\partial \mathcal{V}}{\partial \theta_1} \\ \frac{\partial \mathcal{V}}{\partial \theta_2} \\ \frac{\partial \mathcal{V}}{\partial \theta_3} \end{bmatrix}, \quad \tau = \begin{bmatrix} \tau_1 \\ \tau_2 \\ \tau_3 \end{bmatrix},$$

and the $K(q)$ matrix, that incorporates the effect of holonomic constraint, is defined in (5).

Remark 1. The complete inverse dynamic model $\mathcal{M}_f$ for the Delta robot cannot be expressed in the usual compact form

$$B(q)\ddot{q} + C(q, \dot{q})\dot{q} + g(q) = \tau,$$

where $q = [\theta_1\ \theta_2\ \theta_3]^T$ are the joint variables, $B(q)$ is the inertia matrix, $C(q, \dot{q})$ represents the Coriolis and centrifugal effects and $g(q)$ the
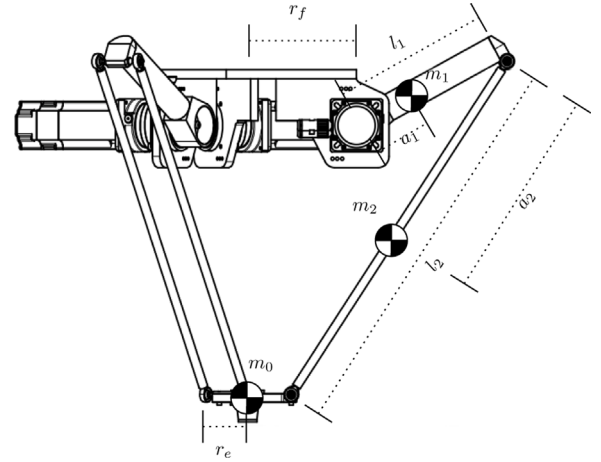

Fig. 5. The CAD model of the D3-1200 Delta Robot. Values of the parameters are listed in Table 1.

gravity term, because of the impossibility of finding a closed form for the passive joint angles ψ_i, γ_i that depends only on the actuated joint angles θ_i for $i \in \{1, 2, 3\}$. A more complex mathematical formulation, including Cartesian and joint variables, given by Eqs. (29) and (30) is thus needed.

4. Experimental setup

This section describes the hardware platform used to perform the experiments for the validation and the comparison of $\mathcal{M}_s$ and $\mathcal{M}_f$ derived in Sections 2 and 3, respectively. A D3-1200 Delta Robot by SIPRO S.r.l. has been used as ground-truth for the generation of the torque profiles. The robot uses an industrial position PID controller to generate the desired torque commands.

A Net Analyzer over Ether-CAT allows the recording of the kinematic information; the command torques and joint positions θ_i are sampled at a frequency of 2 kHz. The joint velocities $\dot{\theta}_i$ and accelerations $\ddot{\theta}_i$ are estimated with a Kalman smoother and the corresponding Cartesian velocities $\dot{x}, \dot{y}, \dot{z}$ and accelerations $\ddot{x}, \ddot{y}, \ddot{z}$ are computed via the robot Jacobian matrix.

To ensure the highest possible accuracy of the estimated torques, the mass values m_i of each component of the robot have been measured with a precision balance, while the length l_i of each link and the position of their respective centers of mass a_i come from their CAD models. Fig. 5 shows the CAD model of the D3-1200 Delta Robot while Tables 1 and 2 list the parameters and their values. The accuracy of the model is evaluated offline by comparing the actual command torques obtained from the D3-1200 Delta Robot with the estimations computed with the mathematical models $\mathcal{M}_f$ and $\mathcal{M}_s$.

We consider three trajectories:

- Y_1 is a pick-and-place trajectory over a belt conveyor, without payload (Fig. 6(a));
- Y_2 consists of the end-effector motion in the middle of the workspace with high and low accelerations (Fig. 6(b)): this trajectory is meant to evaluate the impact of the inertia and Coriolis/centrifugal terms;
- Y_3 is a trajectory that moves the robot and then stops in three target points nearby its workspace limits (Fig. 6(c)): this trajectory is meant to test the model in "extreme" poses.

5. Experimental validation

This section compares the accuracy of the precise model $\mathcal{M}_f$ derived in Section 3 and the simplified model $\mathcal{M}_s$ recalled in Section 2, by
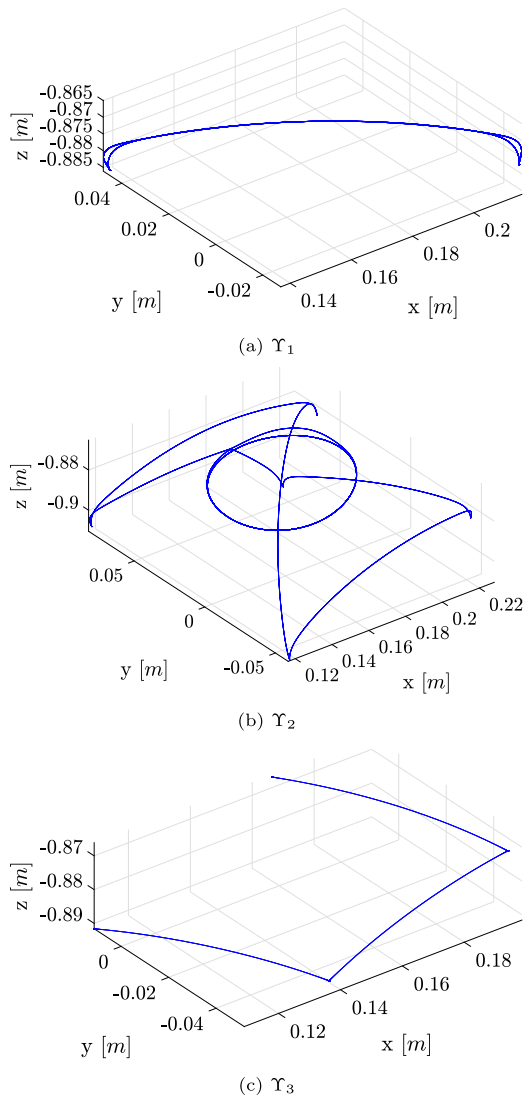
(a) Υ_1

(b) Υ_2

(c) Υ_3

Fig. 6. Experimental validation of the models accuracy on three trajectories. (a) The trajectory Υ_1 is a pick-and-place profile; (b) the trajectory Υ_2 involves high and low accelerations in the center of the workspace; (c) the trajectory Υ_3 moves the robot to its workspace limits.

Table 1
Kinematic and dynamic parameters of D3-1200 delta robot.

Parameter	Value	Unit
r_f	0.25	m
r_e	0.1	m
l_1	0.375	m
l_2	0.9	m
a_1	0.122	m
a_2	0.45	m
m_0	0.94	kg
m_1	1.40	kg
m_2	0.39	kg
$\mathcal{I}_1$	0.035	kg m^2

Table 2
Electromechanical parameters of D3-1200 delta robot.

Parameter	Value
Weight	64 Kg
Power supply	380 V three phase
Motors	Kollmorgen AKM44G (3 units)
Installed power	4.5 KW
Class Protection	IP55
Temperature	$0 \div 45°C$
Humidity	95%
Repeatability	0.1 mm
Max. n° of cycles	150 per minute
DoF	3
Max. working range	1200 mm
Max. payload	4 Kg

Table 3
The means and standard deviations of models of the error for $\mathcal{M}_f$ and $\mathcal{M}_s$ over trajectory Υ_1.

Υ_1	Mean [Nm]			Std [Nm]		
	$\tilde{\tau}_1$	$\tilde{\tau}_2$	$\tilde{\tau}_3$	$\tilde{\tau}_1$	$\tilde{\tau}_2$	$\tilde{\tau}_3$
$\mathcal{M}_f$	0.63	−2.99	−3.77	6.42	7.79	6.61
$\mathcal{M}_s$	10.17	5.74	4.85	11.66	13.23	9.51

Table 4
The means and standard deviations of the errors for models $\mathcal{M}_f$ and $\mathcal{M}_s$ over trajectory Υ_2.

Υ_2	Mean [Nm]			Std [Nm]		
	$\tilde{\tau}_1$	$\tilde{\tau}_2$	$\tilde{\tau}_3$	$\tilde{\tau}_1$	$\tilde{\tau}_2$	$\tilde{\tau}_3$
$\mathcal{M}_f$	2.41	−1.43	−2.18	14.27	12.62	11.60
$\mathcal{M}_s$	12.13	7.25	6.02	27.72	23.74	23.87

5.1. Model accuracy

Υ_1 aims to evaluate the models in the most frequent task of the robot: it consists in rapid movements between two belt conveyors combined with a mono-directional vertical movement used to pick an object.

From the torque profiles in Fig. 7, it is possible to notice how the simplified model $\mathcal{M}_s$ underestimates the control torque profiles. Moreover, during a pick action, i.e., when the accelerations are small, the simplified model predicts an almost constant negative offset. The precise model $\mathcal{M}_f$ has a much more accurate estimation of the command torques. When the robot moves the end-effector from one conveyor belt to the other, i.e, when the trajectory has the highest dynamics, the torque peaks of $\mathcal{M}_f$ are close to the actual ones.

To evaluate the precision of each model, we consider the errors $\tilde{\tau}_i^f$, $\tilde{\tau}_i^s$ between the estimates $\hat{\tau}_i^f$, $\hat{\tau}_i^s$ for $\mathcal{M}_f$ and $\mathcal{M}_s$ and the actual commands τ_i

$$\tilde{\tau}_i^f = \tau_i - \hat{\tau}_i^f,$$
$$\tilde{\tau}_i^s = \tau_i - \hat{\tau}_i^s.$$

Fig. 10(a) and Table 3 report the mean and the standard deviation of the torque errors. The bar-plot allows to notice the reduction of the error of $\mathcal{M}_f$ with respect to the model $\mathcal{M}_s$.

The trajectory Υ_2 is meant to evaluate the behavior of the model when subjected to high and low accelerations in the middle of the robot workspace. In particular, this trajectory is similar to pick-and-place operations which took place between 5 to 10 centimeters apart from the center of the workspace as shown in Fig. 6(b). The torque profiles in Fig. 8 show the improvements of $\mathcal{M}_f$ with respect to $\mathcal{M}_s$, especially during motion generated by high torque values.
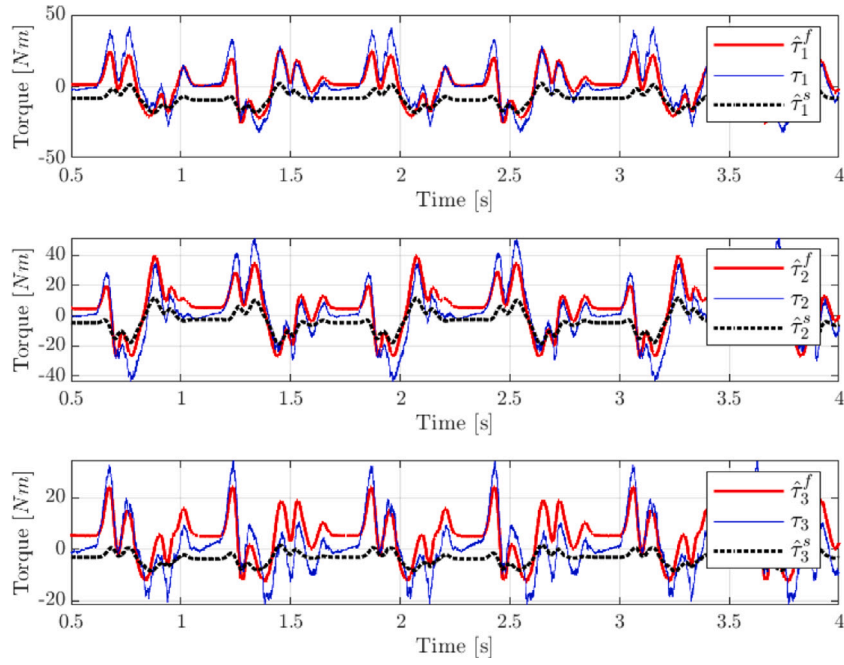
using the data collected as explained in the previous section. Moreover, we provide a complexity analysis to evaluate the trade-off between accuracy and computational complexity.

Fig. 7. Actual Torques (blue line) τ_i compared with estimated torques $\hat{\tau}_i^f$ computed by $\mathcal{M}_f$ (red line) and the estimated torques $\hat{\tau}_i^s$ computed by $\mathcal{M}_s$ (dotted line), for each actuated joint using the trajectory Y_1 showed in Fig. 6(a). (For interpretation of the references to color in this figure legend, the reader is referred to the web version of this article.)

Fig. 8. Actual Torques (blue line) τ_i compared with estimated torques $\hat{\tau}_i^f$ computed by $\mathcal{M}_f$ (red line) and the estimated torques $\hat{\tau}_i^s$ computed by $\mathcal{M}_s$ (dotted line), for each actuated joint using the trajectory Y_2 showed in Fig. 6(b). (For interpretation of the references to color in this figure legend, the reader is referred to the web version of this article.)
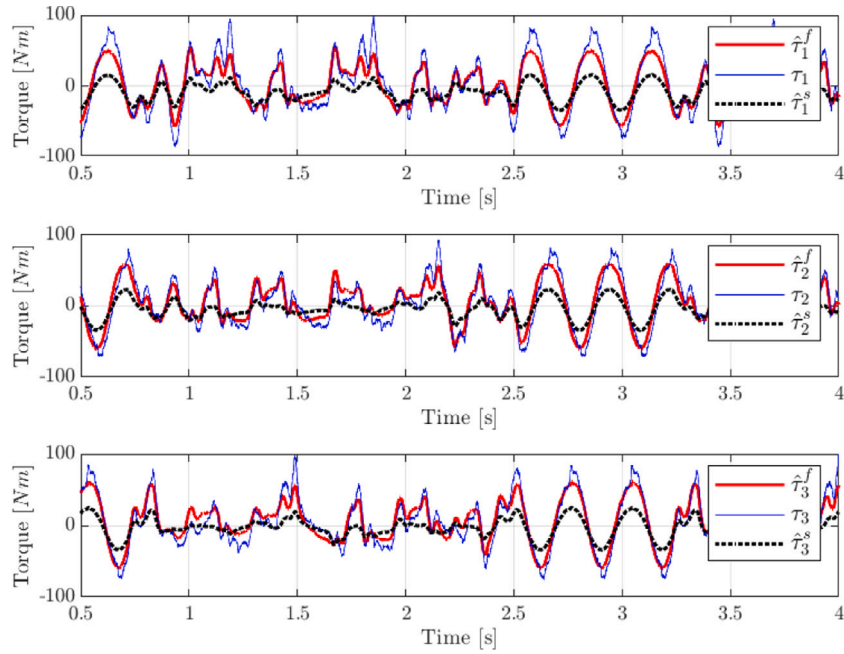
When the robot operates around the center of the workspace, the model $\mathcal{M}_s$ performs better than in the previous experiment: indeed, it predicts with higher accuracy when the accelerations are high with fast changes of directions (i.e., between $2.5s$ and $3.25s$), and the profiles are quite close to the actual ones. On the other hand, it underestimates the torques during the pick-and-place motion (i.e. between $0.75s$ and

$2.25s$). The model $\mathcal{M}_f$ provides a better estimation of the torques over the whole duration of the trajectory. Fig. 10(b) and Table 4 show the mean and the standard deviation of the estimation errors.

Y_3 aims to evaluate accuracy when the robot motion alternates from high and slow dynamics. The trajectory consists of high accelerations toward poses on the boundary of the workspace, followed by constant
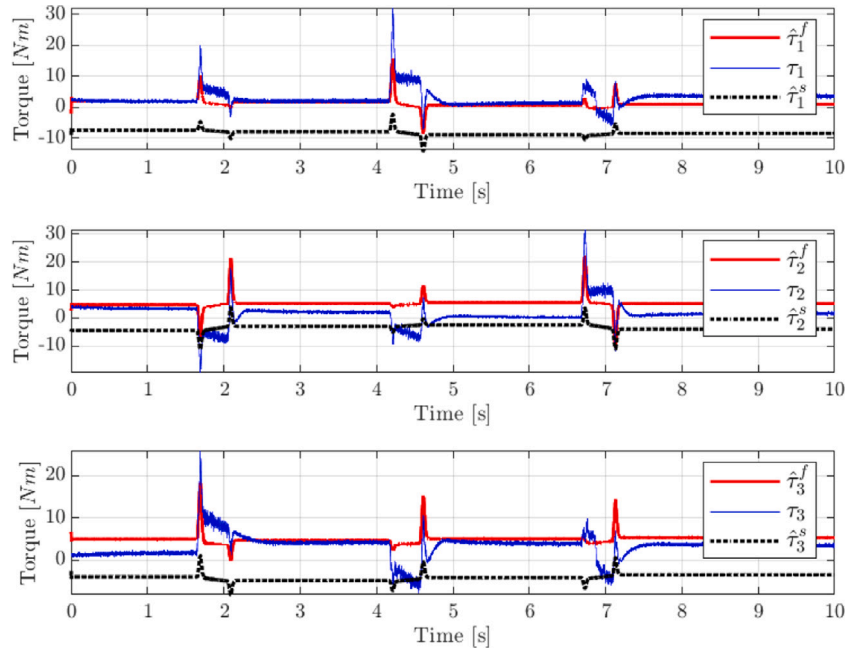
Fig. 9. Actual Torques (blue line) τ_i compared with estimated torques $\hat{\tau}_i^f$ computed by $\mathcal{M}_f$ (red line) and the estimated torques $\hat{\tau}_i^s$ computed by $\mathcal{M}_s$ (dotted line), for each actuated joint using the trajectory Υ_3 showed in Fig. 6(c). (For interpretation of the references to color in this figure legend, the reader is referred to the web version of this article.)
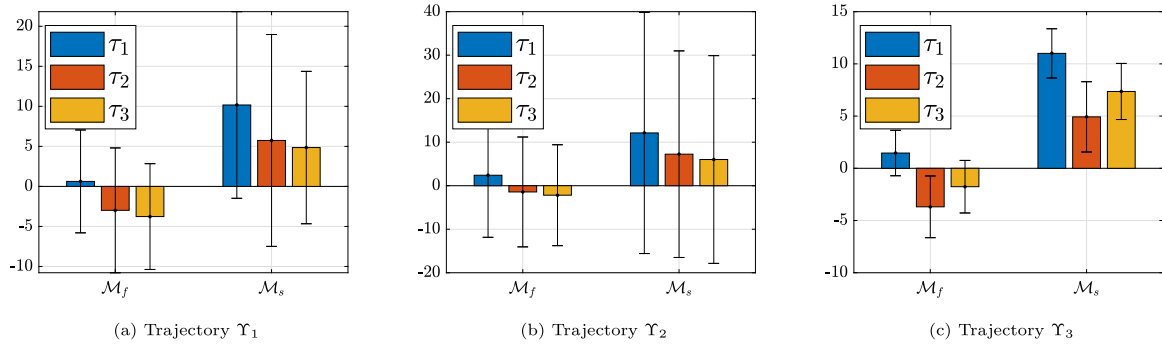

Fig. 10. Torque mean errors with standard deviation bars for models $\mathcal{M}_f$ and $\mathcal{M}_s$.

Table 5
The means and standard deviations of the errors for models $\mathcal{M}_f$ and $\mathcal{M}_s$ over trajectory Υ_3.

Υ_3	Mean [Nm]			Std [Nm]		
	$\bar{\tau}_1$	$\bar{\tau}_2$	$\bar{\tau}_3$	$\bar{\tau}_1$	$\bar{\tau}_2$	$\bar{\tau}_3$
$\mathcal{M}_f$	1.46	−3.69	−1.76	2.17	2.95	2.52
$\mathcal{M}_s$	11.01	4.93	7.36	2.36	3.37	2.68

poses for a few seconds. The trajectory allows to test the accuracy of the model outside the usual working area.

Fig. 9 shows that the model $\mathcal{M}_s$ has a significantly large error when the robot is near the workspace limit. The torque peaks during the motion between the target points are not correctly computed and most of the time are underestimated. $\mathcal{M}_f$ is more accurate, both during static and dynamic parts. Means and standard deviations of the errors are shown in Fig. 10(c) and listed in Table 5.

The remaining errors between the command torques calculated by $\mathcal{M}_f$ and the actual torques applied to the D3-1200 Delta Robot are

due to different phenomena that are not taken into consideration in our model in order not to make it too complex. The main terms not modeled are: joints flexibility, links flexibility, friction at the joints, non-linearity of the gear-boxes, dynamic model of the electric motors. Moreover, it is worth mentioning that in our model we used the values for the parameters given by the CAD models. It is possible that such values are not precise.

Remark 2. An alternative method to increase precision in computing the torque profiles and keep an acceptable computational burden could be the approach proposed in [13], in which the simplified model $\mathcal{M}_s$ is improved by embedding two parameters on the inertia and potential energy. The optimal values of such parameters are calculated through gray-box identification on actual data. The final inverse dynamic model has shown better precision and quick computation. The major drawback is that the parameters are strictly related to the specific robot. Therefore, the complete model $\mathcal{M}_f$ presented in this work has the advantage of using the dynamic parameters of the Delta robot from CAD design.

vẫn nên promote một phương pháp đính kèm estimator để compensate cho các thông số friction và gearbox để tăng độ chính xác

Table 6

Number of operations executed in the full and simplified inverse dynamic model.

	Number of operations					
	+	−	×	÷	sin	cos
$\mathcal{M}_s$	50	27	79	6	7	9
$\mathcal{M}_f$	669	477	2029	2016	12	15

Table 7

The average and maximum frequency obtained by computing the torque profile over a large set of trajectory for the models $\mathcal{M}_s$ ans $\mathcal{M}_f$.

	Avg frequency [kHz]	Max frequency [kHz]
$\mathcal{M}_s$	32.10	35.97
$\mathcal{M}_f$	4.65	5.02

5.2. Model complexity

An inverse dynamics based control is used to obtain better performance than with standard PID controllers. When the dynamic model is involved in the control loop, the equations of motion must be solved at high frequency to provide the feedforward control torques. The experiments in the previous subsections shown the better accuracy of $\mathcal{M}_f$ compared to the simplified $\mathcal{M}_s$.

The study of the computational complexity of the two models $\mathcal{M}_f$ and $\mathcal{M}_s$ addressed in this section is evaluated in terms of time complexity in the worst case scenario, which involves the usage of processors which do not have integrated ALU and the usage of not optimized algorithms for the computation of the binary operations. The time complexity is computed by multiplying the number of basic operations with the complexity of the operations. Given two n-digit numbers, the complexity for the addition and subtraction is $O(n)$ using the addition with carry and subtraction with borrow algorithms. The complexity for multiplication and division, using standard algorithms is $O(n^2)$. Trigonometric functions as sine and cosine are constructed by composing arithmetic functions; in particular exploiting the Taylor series, with repeated argument reduction and direct summation we obtain a time complexity of $O(n^{5/2})$. The number of executed scalar operations, counted from the C++ implementation of both models, is reported in Table 6. According to the table the time complexity of $\mathcal{M}_s$ is

$$O(77n + 85n^2 + 16n^{5/2}),$$

while the time complexity of $\mathcal{M}_f$ is

$$O(1176n + 4045n^2 + 27n^{5/2}).$$

Thus, both models can be computed in polynomial time.

As expected the coefficients that multiply n and n^2 for $\mathcal{M}_f$ are larger than the coefficients for $\mathcal{M}_s$. We performed an analysis on the maximum and average execution frequency for both models in order to experimentally evaluate the impact of the coefficients for $\mathcal{M}_s$ and $\mathcal{M}_f$ on the computational burden. The computer has a single-core CPU operating at 2.5 GHz. We calculated the torques with both models, over a set of different trajectories, as reported in Table 7. It turns out that $\mathcal{M}_f$ has a negative speed-up of 0.1449 on the average frequency. It still has to be considered that $\mathcal{M}_f$ has an average control loop that reaches frequencies higher than 4 kHz, which is still a high computation rate for modern controllers. Thus, despite the negative speed-up, $\mathcal{M}_f$ is totally suitable to be used within controllers of Delta Robots.

6. Conclusions

A mathematically rigorous inverse dynamic model for industrial Delta Robots, obtained by adopting the Euler–Lagrange approach, has been presented. The model has been validated through a direct comparison with real torque profiles of an industrial Delta Robot. The proposed model has been tested and verified over a set of trajectories which covers the most common and stressful tasks, and proved to be more accurate than state-of-art counterparts.

The increased computational complexity has been analyzed and confirmed to be larger than state-of-art counterparts, but it does not compromise the implementation in real-time industrial controllers.

The model does not need any parameter identification, making it ready for direct use into a robot controller, and it is adaptable to any 3-DoF Delta Robot of which the kinematic and dynamic parameters are known.

CRediT authorship contribution statement

Fabio Falezza: Software, Validation, Investigation, Formal analysis, Writing – original draft, Visualization. **Federico Vesentini:** Conceptualization, Methodology, Software, Validation, Formal analysis, Writing – review & editing. **Alessandro Di Flumeri:** Data curation. **Luca Leopardi:** Data curation. **Gianni Fiori:** Data curation. **Gianfrancesco Mistrorigo:** Data curation. **Riccardo Muradore:** Conceptualization, Supervision, Project administration.

Declaration of competing interest

The authors declare that they have no known competing financial interests or personal relationships that could have appeared to influence the work reported in this paper.

References

[1] Wu J, Wang J, Wang L, Li T. Dynamics and control of a planar 3-DOF parallel manipulator with actuation redundancy. Mech Mach Theory 2009;44(4):835–49.

[2] Wu J, Yu G, Gao Y, Wang L. Mechatronics modeling and vibration analysis of a 2-DOF parallel manipulator in a 5-DOF hybrid machine tool. Mech Mach Theory 2018;121:430–45.

[3] Wu J, Zhang B, Wang L, Yu G. An iterative learning method for realizing accurate dynamic feedforward control of an industrial hybrid robot. Sci China Technol Sci 2021;1–12.

[4] Staicu S, Carp-Ciocardia D-C. Dynamic analysis of clavel's delta parallel robot. In: IEEE international conference on robotics and automation. Vol. 3. 2003, p. 4116–21.

[5] Bortoff SA. Object-oriented modeling and control of delta robots. In: IEEE conference on control technology and applications. 2018, p. 251–8.

[6] Clavel R. Dispositif pour le déplacement et le positionnement d'un élément dans l'espace. Google Patents. 1987.

[7] Pierrot F, Nabat V, Company O, Krut S, Poignet P. Optimal design of a 4-DOF parallel manipulator: From academia to industry. IEEE Trans Robot 2009;25(2):213–24.

[8] Pierrot F, Dauchez P, Fournier A. HEXA: a fast six-DOF fully-parallel robot. In: Fifth international conference on advanced robotics' robots in unstructured environments. IEEE; 1991, p. 1158–63.

[9] Brinker J, Corves B, Wahle M. A comparative study of inverse dynamics based on clavel's delta robot. In: Proceedings of the 14th world congress in mechanism and machine science. Taipei, Taiwan; 2015, p. 25–30.

[10] Kuo Y-L. Mathematical modeling and analysis of the delta robot with flexible links. Comput Math Appl 2016;71(10):1973–89.

[11] Stamper RE. A three degree of freedom parallel manipulator with only translational degrees of freedom (Ph.D. thesis), 1997.

[12] Park SB, Kim HS, Song C, Kim K. Dynamics modeling of a delta-type parallel robot. In: IEEE ISR. 2013, p. 1–5.

[13] Falezza F, Vesentini F, Di Flumeri A, Fiori G, Mistrorigo G, Muradore R. Gray-box model identification and payload estimation for delta robots. In: 2020 IFAC world congress. 2020.

[14] Angel L, Viola J. Parametric identification of a delta type parallel robot. In: IEEE colombian conference on robotics and automation. 2016, p. 1–6.

[15] Ahmadi M, Dehghani M, Eghtesad M, Khayatian AR. Inverse dynamics of hexa parallel robot using lagrangian dynamics formulation. In: 2008 International conference on intelligent engineering systems. IEEE; 2008, p. 145–9.

[16] Miller K, Clavel R. The Lagrange-based model of delta-4 robot dynamics. Robotersysteme 1992;8(1):49–54.

[17] Angel L, Sebastian J, Saltaren R, Aracil R. Robotenis system part II: Dynamics and control. In: Proceedings of the 44th IEEE conference on decision and control. IEEE; 2005, p. 2030–4.

[18] Kenmochi M, Avci E, Kawanishi M, Narikiyo T, Kawakami S, Saitou Y. Robust position control of delta parallel mechanisms using dynamic model and QFT. In: 2014 IEEE 23rd international symposium on industrial electronics. IEEE; 2014, p. 1256–61.

[19] Asadi F, Heydari A. Analytical dynamic modeling of delta robot with experimental verification. Proc Inst Mech Eng K J Multi Body Dyn 2020.

[20] Siciliano B, Sciavicco L, Villani L, Oriolo G. Robotics: modelling, planning and control. Springer Science & Business Media; 2010.

[21] Clavel R. Conception d'un robot parallèle rapide à 4 degrés de liberté. Tech. rep. EPFL, 1991.

[22] Kuo Y-L, Huang P-Y. Experimental and simulation studies of motion control of a delta robot using a model-based approach. Int J Adv Robot Syst 2017;14(6):1–14.

[23] Tsai L-W. Robot analysis: the mechanics of serial and parallel manipulators. John Wiley & Sons; 1999.

[24] Bullo F, Lewis AD. Geometric control of mechanical systems: modeling, analysis, and design for simple mechanical control systems. Vol. 49. Springer; 2019.

Federico Vesentini received the B.S. and M.S. degrees in applied mathematics from the University of Verona, Verona, Italy in 2013 and 2017, respectively. He is currently a Ph.D. student at the University of Verona. His research interests focus on modeling hybrid systems for mobile robots and collision-free trajectory planning.